TIME DOMAIN MODELLING OF UWB GPR AND ITS APPLICATION ON LANDMINE DETECTION

B. Scheers, M. Acheroy
ELTE Dep., Royal Military Academy
30, Avenue de la Renaissance B-1000 Brussels
bart.scheers@elec.rma.ac.be, marc.acheroy@elec.rma.ac.be

A. Vander Vorst
Hyperfréquences U.C.L., Belgium
vandervorst@emic.ucl.ac.be

ABSTRACT

In this paper, the time domain modelling of an indoor impulse UWB GPR systems (1GHz-5GHz), built in the scope of the HUDEM project, is presented. For an impulse UWB system, a time-domain modelling is an obvious choice. We explain how the antennas can be characterised by their normalised impulse response. By considering the antenna as a convolution operator, we get a mechanism for modelling the whole radar system as a cascade of linear responses, which gives a lot of advantages and possible application. In our research it is used to express the radar range equation in the time-domain, to optimise the antenna configuration and to calculate the point-spread function of the UWB GPR at a given depth. The point-spread function can be used for migration by deconvolving it from the collected data. In this way the migration method takes into account the characteristics of the radar system. Finally, results of this migration method on data obtained by our UWB GPR system are shown.

Keywords: Humanitarian demining, UWB GPR, time domain modelling, migration.

1. INTRODUCTION

The Ground Penetrating Radar is a promising technology for detection and identification of buried landmines. As landmines are small objects and often shallow laid, a large bandwidth is needed for a better depth resolution and detailed echo. The use of impulse wideband systems involves some technical problems. Critical points are the UWB antennas and the receiver.

At the start of the HUDEM project in 1996, we decided to build an indoor time-domain UWB GPR (1GHz-5GHz), to study the advantages and shortcomings of such a system. The system components are, except for the antennas, mainly off-the-shelf equipment. It consists of the following parts: on the transmitting side a Gaussian impulse generator is used. The generated impulse has a maximal amplitude of 2.5 Volts and a FWHM of less than 100 ps. On the receiver side, a 6GHz digitising oscilloscope is used to measure the backscattered signal. The oscilloscope has an internal delay line, a 14 bit resolution and can average up to 10000 times, to obtain a higher dynamic range. The antenna pair consists of two TEM horn antennas and is mounted on a computer-controlled xy-table of 2m by 2.5m and 2m high. In the scanning area of the table, two boxes are placed, 1.5m by 1.5m each and 0.8m deep. The first one is filled with sand, the second one with loam. The permittivity of both types of soil is fully characterised in function of frequency and moisture content.

The main effort was put in the development of directive UWB TEM horn antennas [1] that can be used off-ground. In the design of the TEM horns we tried to limit the dimensions and weight of the antennas to guarantee a high degree of mobility. To reduce the physical size of the antennas and to improve the directivity, without reducing too much the bandwidth, the antennas were filled with a dielectric ($\boldsymbol{e}_r \approx 3$). The TEM horns were designed to match the $50\,\Omega$ driving cable. To avoid reflection of an unbalanced current component on the coax feedline exterior, a wideband balun was integrated [2].

2. ANTENNAS AS CONVOLUTION OPERATORS

A common way of describing antennas in the time domain is by means of their impulse response (IR). Different types of IRs can be defined. We opted for the normalised impulse response (normalised IR), i.e. an impulse response integrating all frequency dependent antenna characteristics [3], [4]. In this way, the time domain antenna equations, expressed in terms of the normalised IR, become very simple and accurate to use. No assumptions about frequency dependent terms has to be made. To simplify the expressions, we only consider antenna performance for dominant linear polarisation of the E-field. The extension to the more general case is possible.

First consider the time-domain antenna equation for the transmitting antenna. The co-ordinates system is given on Fig.1, the origin $\vec{r} = 0$ is taken in the virtual source of the antenna, i.e. an apparent point in the antenna from which the radiated field degrades by a factor $1/r$. The radiated field in the far field is given by:

$$E_{rad}(r, \boldsymbol{q}, \boldsymbol{j}, t) = \frac{1}{2\boldsymbol{p}\, rc} h_{N,Tx}(\boldsymbol{q}, \boldsymbol{j}, t) \otimes \frac{\sqrt{Z_0}}{\sqrt{Z_c}} \frac{dVs(t - r/c)}{dt} \tag{1}$$

$h_{N,Tx}(\boldsymbol{q}, \boldsymbol{j}, t)$ is the normalised IR of the transmitting antenna in the direction $(\boldsymbol{q}, \boldsymbol{j})$, $V_S(t)$ is the excitation voltage at the antenna feed in a 50 Ω load, Z_c the impedance of the feed cable, Z_0 the impedance of free space, and c the speed of light. The operator $\otimes$ denotes a convolution in the time.
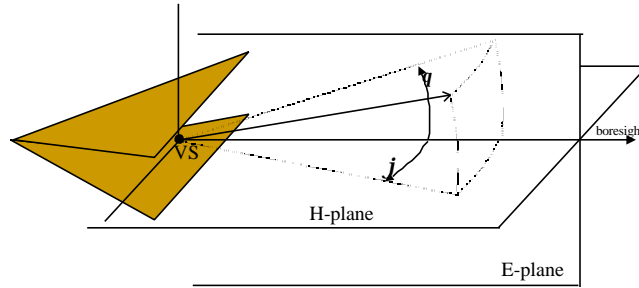

Fig 1: TEM horn antenna and co-ordinate system for the time-domain antenna equations.

Consider now the same antenna as a receiving antenna. The received voltage $V_{rec}(t)$, in a 50 Ω load, at the feed of the antenna for an incoming field $E_{inc}(\vec{r} = 0, t)$, evaluated in the virtual source of the antenna and with an incident direction $(\boldsymbol{q}, \boldsymbol{j})$, is given by:

$$V_{rec}(t) = \frac{\sqrt{Z_c}}{\sqrt{Z_0}} h_{N,Rx}(\boldsymbol{q}, \boldsymbol{j}, t) \otimes E_{inc}(\vec{r} = 0, t) \tag{2}$$

The two time-domain antenna equations (1) and (2) are defined in such a way that $h_{N,Tx} = h_{N,Rx}$ for two identical antennas. It is seen that within the 3dB beamwidth of the antennas, the normalised IR can be expressed as $h_N(\boldsymbol{q}, \boldsymbol{j}, t) = k.h_N(0,0,t)$, with $h_N(0,0,t)$ the normalised IR on boresight of the antenna and k the peak voltage pattern of the antenna in the direction $(\boldsymbol{q}, \boldsymbol{j})$. Hence the antennas are completely characterised by the two latter. The normalised IR on boresight is easy to measure, using two identical antennas and a vector network analyser [4]. Fig. 2 shows the normalised IR on boresight of the antennas designed for the laboratory UWB GPR.
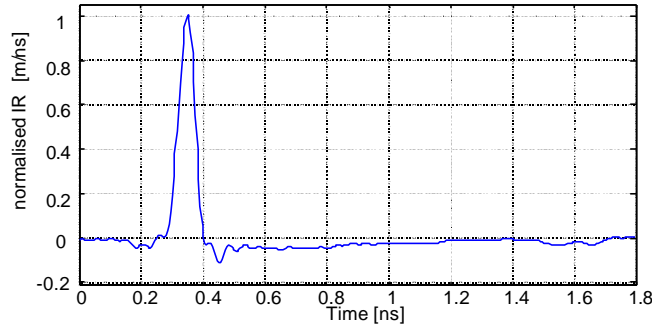
Fig.2: Normalised IR of TEM horn antenna

One of the advantages of considering the antenna as a convolution operator is that we get a mechanism for modelling the whole radar system as a cascade of linear responses.

3. RANGE PERFORMANCE OF THE SYSTEM

The radar range equation is a useful description of the factors influencing radar performance. Describing performances of an "impulse" system, using the radar range equation in the frequency domain, has some drawbacks: it contains frequency dependent terms and does not specify the nature of the transmitted signal. Furthermore, it is more convenient to state the minimum detectable signal of a time-domain system as a peak voltage instead of frequency dependent signal power. Expressing the radar range equation as a cascade of impulse responses would be more practical. Consider an electromagnetic configuration as shown on Fig. 3:

$\vec{i}_r = \dfrac{\vec{r}'-\vec{r}}{\left|\vec{r}'-\vec{r}\right|}$ is a unit vector pointing from the transmitting antenna at co-ordinate $\vec{r}$ towards the target located at $\vec{r}'$.

$\vec{i}_i = \dfrac{\vec{r}''-\vec{r}'}{\left|\vec{r}''-\vec{r}'\right|}$ is a unit vector pointing from the target towards the receiving antenna located at $\vec{r}''$.

The backscattered field from the target, characterised by an IR $\Lambda_{v,v}(\vec{i}_r,\vec{i}_i,t)$, can be described as:

$$E_{scat}(\vec{r}'',t) = \frac{1}{4p\left|\vec{r}''-\vec{r}\right|}\Lambda_{v,v}(\vec{i}_r,\vec{i}_i,t)\otimes E_{rad}(t-\left|\vec{r}''-\vec{r}\right|/c) \tag{3}$$

The time vector $\Lambda_{v,v}(\vec{i}_r,\vec{i}_i,t)$ only takes into account the backscattered signal in the same polarisation as the incoming field and is the time equivalent of the square root of the target radar cross section.

Further some additional losses have to be introduced. In the scope of demining applications, using antennas off-ground, we will only take into account the transmission losses at the air-ground interface and the propagation loss in the ground. The transmission losses at the air-ground interface are given by the two oblique incident transmission coefficients T_{trans} and $T_{retrans}$ on the interface. The propagation losses in the ground are not so easy to introduce. The best way to handle with these losses is representing the ground as a low-pass filter. The transfer function of this filter, representing a propagation of d meters in the ground, is given by $H_d(w) = e^{-(a+jb)d}$, where α is the attenuation constant [Np/m] of the medium and β the phase constant [rad/m]. Both constants are function of frequency and complex permittivity $e' - je''$. For a given soil, i.e. texture, density and moister content, and for a given two-way path length d in the ground, the impulse response $g_d(t)$ of the soil, representing the propagation losses, can be calculated. Substituting equation (1), (2) and (3), and introducing the additional losses, the GPR radar range equation in the time-domain is found as:

$$V_{rec}(t) = \frac{T_{trans} T_{retrans}}{8p^2 R_t R_r c} \cdot g_d(t) \otimes h_{N,Tx}(\vec{i}_r,t) \otimes \Lambda_{v,v}(\vec{i}_r,\vec{i}_i,t) \otimes h_{N,Rx}(-\vec{i}_i,t) \otimes \frac{dVs(t)}{dt} \qquad (4)$$

With R_t : The total path length from transmitting antenna to the target

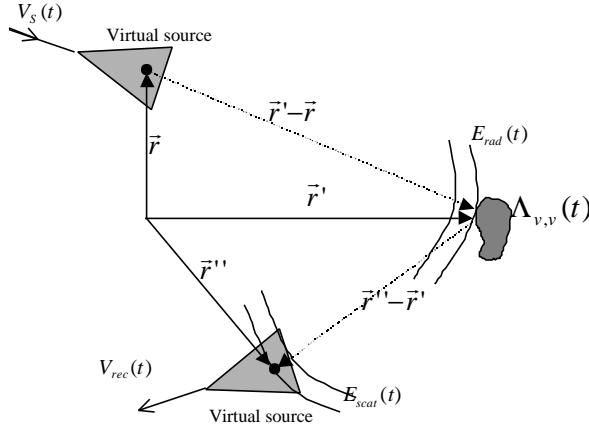R_r : The total path length from receiving antenna to the target

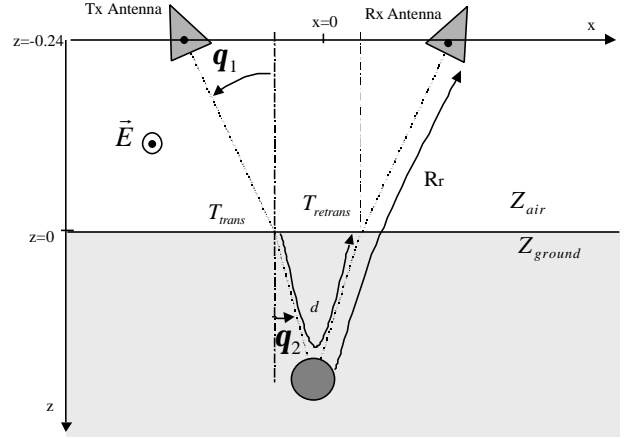Fig. 3: Electromagnetic configuration

Fig. 4: Configuration of UWB GPR

The losses due to the off-boresight position of the target are already taken into account by $h_N(\vec{i},t)$.

Fig. 5 shows the range performance of our laboratory UWB system for a fictitious metallic target in a lossy rice field soil. The soil, coming from Cambodia, has a texture composition of 69% of sand, 24% of silt and 7% of clay. This sandy soil represents a regular agriculture soil with which deminers are confronted. The complex permittivity of the soil was measured in function of the moister content over a large frequency band. The target is a fictitious metallic object with an IR $\Lambda_{v,v}(t) = 0,314.d(t)$, comparable to an IR of a metallic sphere with a radius of 50 mm, taking only into account the surface scattering. In the implementation, we introduced some approximations and simplifications, without loss of generality: the bistatic RCS of the target is taken independent of the bistatic angle, the antennas are always focussed on the target and the transmission coefficients suppose a flat interface and a polarisation parallel to the interface. The virtual sources of the antennas are at 24 cm above the ground and the two antennas are separated by 22.8 cm (Fig. 4). The air-ground interface is at z=0.

The minimal detectable peak amplitude of our receiver, limited by its noise performance and the antenna coupling, is about 1 mV (-47 dBm). This means that the maximal depth of the target to be detected in a 10% moister soil is 10 cm. It can be seen that the performance of an UWB system is limited by the moister content of the soil. Note that the driving source $V_S(t)$ of the laboratory system has a maximum amplitude of only 2.5 V and that the receiver has a 14 bit resolution and no time varying gain. Another impulse generator and receiver could enhance the range performance.
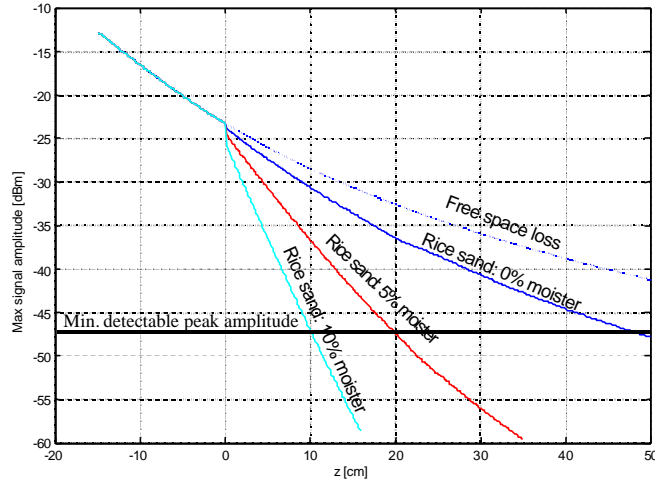
Fig. 5: Peak amplitude of the reflection on the target [dBm] in function of z [cm] for 0%, 5% and 10% moister content.

4.   **ANTENNA CONFIGURATION**

In the design of the laboratory UWB GPR, a study was made to optimise the position and orientation of the Tx and Rx antennas. To reduce the coupling between the two TEM horns, they were put side by side with a common H-plane. In principle antenna coupling is not critical and can be compensated for, but if the ringing between the two antennas lasts too long, it can interfere with the useful backscattered signal. The height of the antennas above the ground is chosen to be around 25 cm.

An important parameter for the Tx-Rx antenna configuration is the combined antenna pattern – i.e. the pattern of the two antennas considered as one antenna. The resulting 3dB beamwidth of this combined antenna pattern is obviously a function of the offset angle q_1 as represented on Fig. 6a. A large 3dB beamwidth is not a priori unfavorable. When scanning over a point target with the GPR, the B-scan will show a hyperbolic structure in the reflection (Fig. 6b). A larger 3dB beamwidth produces larger hyperbolas in the B-scan, and can therefore increase the detectability of objects. As a criterion for the optimisation of this offset angle q_1, we have considered the total energy found in the hyperbolic shaped response of a point target. This total energy represents in some sense the expected reflected energy of the point target, after enhancing the B-scan by an optimal migration method. For this reason, we simulated different synthetic B-scans (Fig. 6b) of a point scatterer at 6 cm in the ground, for different values of q_1. The fictitious point scatterer is represented by a bistatic impulse response $\Lambda_{v,v} = d(t)$. For each position x of the antenna pair (Fig 5a), the backscattered signal $V_{rec}(t)$ was calculated using the radar range equation (4).
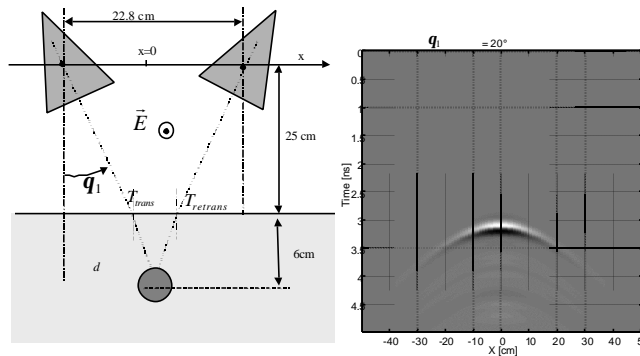

Fig. 6a: Antenna configuration   Fig. 6b: synthetic B-scan

The total energy in the hyperbolic shaped response of the target is calculated as $E_{tot} = \int\limits_{x} \int\limits_{t} |V_{rec}(t)|^2 \, dt \, dx$. Fig. 7 shows the total energy in the hyperbolic response of the point target as a function of the offset angle q_1. The maximal energy in the hyperbola is found for an offset angle of 20°, which for this configuration (object at a depth of 6 cm) corresponds to the angle that focuses the antennas on the target, taking into account the refraction. In reality the depth of the object is a priori unknown, but is expected to be between 0 and 20 cm. Therefore, in the design of the laboratory UWB GPR, an angle q_1 of 20° was chosen.
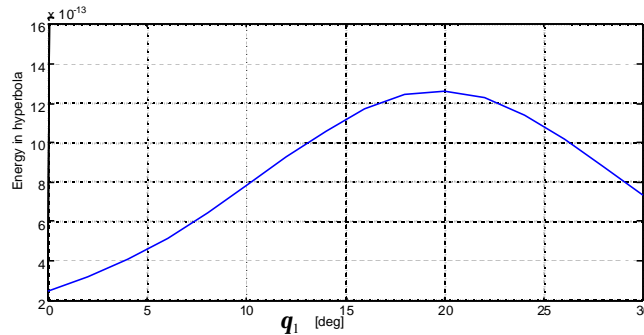

Fig. 7: Total energy in the hyperbolic shaped response of a point target at 6 cm of depth.

5. MIGRATION BY SPACE-TIME DECONVOLUTION

In the data recorded by the UWB GPR system, we expected additional information on the targets thanks to the larger system bandwidth. However, signal-processing techniques on the A-scans, essentially based on Prony methods and on time-frequency analysis, were applied without much success. This is probably due to the low Q factor of the mine-like targets. None of these methods seems to be robust enough for target classification purposes. For this reason the signal processing work was reoriented towards the processing of the 3D data (C-scans), trying to extract more information on the shape of the buried objects. To enhance the spatial resolution of the recorded data, migration techniques are used.

Migration is a common name for processing techniques that try to reconstruct, from the data recorded at the surface, the reflecting structures in the sub-surface. Due to the beam-width of transmit and receive antenna, the reflections on structures will be smeared out over a broad region in the recorded data, and will appear as hyperbolic structures. The aim of migration techniques is to focus target reflections in the recorded data back into their true position and physical shape. In this respect, migration can be seen as a form of spatial deconvolution that increases spatial resolution. A good overview of migration techniques is given in [5] and [6]. In most of the migration techniques, the characteristics of the GPR system, like antenna patterns, impulse response of the antennas, the waveform of the source, … etc, are not included. In this section we present a migration method that takes into account the system characteristics and eventually the ground characteristics. The migration scheme is based on the deconvolution of the recorded data with the point-spread function of the system. As in a lot of migration algorithms, it is assumed that the interaction between the scatterers present in the scene is totally neglected.

The migration by deconvolution has only sense if the acquisition process by the UWB GPR is a convolution between the structures present in the subsurface and the point-spread function of the system. This is true under certain assumptions. Suppose for simplicity a monostatic antenna configuration. The medium can only have a propagation velocity variation in the downward direction. The antennas are moved in a xy-plane at $z = 0$. The 3D data, $V_{rec}(x, y, z = 0, t)$ is taken on a rectangular grid with spacing Δx and Δy. Assume in a first step there is a point-target present in the subsurface located at $\vec{r}_o = (x_o, y_o, z_o)$, characterized by an IR $\Lambda_o(\vec{r}_o, t_o)$, independent of the incident direction and not necessarily a dirac impulse. For the antennas at any position $\vec{r}_a = (x_a, y_a, z = 0)$, the received voltage can be written using (4) as:

$$V_{rec}(\vec{r}_a, t) = \frac{1}{8p^2 |\vec{r}_o - \vec{r}_a|^2 v} \cdot g_d(t) \otimes h_{N,Tx}(\vec{i}_r, t) \otimes \Lambda_o(t - \frac{2|\vec{r}_o - \vec{r}_a|}{v}) \otimes h_{N,Rx}(-\vec{i}_r, t) \otimes \frac{dVs(t)}{dt} \tag{5}$$

By grouping all the factors, except the IR of the point-target, in a factor $s(\vec{r}_a, \vec{r}_o, t)$, equation (5) becomes:

$$V_{rec}(\vec{r}_a, t) = s(\vec{r}_a, \vec{r}_o, t) \otimes \Lambda_o(t) \tag{6}$$

$s(\vec{r}_a, \vec{r}_o, t)$ represents the voltage response of a point scatterer placed in $\vec{r}_o$ with IR $d(t - \frac{|\vec{r}_a - \vec{r}_o|}{v})$, as a function of the antenna position $\vec{r}_a$ and time t. Further, for the antennas at $z = 0$ and the point scatterer at $z = z_o$, the response $s(\vec{r}_a, \vec{r}_o, t)$ is a function of $\vec{r}_o$ and $\vec{r}_a$ only by their difference. Note that the convolution in equation (6) is a convolution in the time. If an object can be modelled by a set of independent point targets all at approximately the same depth $z = z_o$, the resulting voltage $V_{rec}(\vec{r}_a, t)$ will be a linear combination of the voltage responses of each individual point target and can be expressed as:

$$V_{rec}(x_a, y_a, t) = \iint_{x,y} \int_t s(x_a - x, y_a - y, z_o, t - t)\Lambda_{zo}(x, y, t)dt\, dxdy \tag{7}$$

Equation (7) represents a space-time convolution along the co-ordinates x, y and t, and can be written as:

$$V_{rec}(x, y, t) = s_{z_o}(x, y, t) \otimes \Lambda_{zo}(x, y, t) \tag{8}$$

Where $\Lambda_{zo}(x, y, t)$ is a 3D image containing the responses, associated with the distributed targets at the positions (x, y, z_o). The 3D matrix $s_{z_o}(x, y, t)$ represents the point-spread function of the UWB GPR system for a depth $z = z_o$ and is calculated using (5) for different antenna positions $\vec{r}_a$ and a point scatterer with IR $d(t - \frac{|\vec{r}_a - \vec{r}_o|}{v})$. Although the point-spread function $s_{z_o}(x, y, t)$ is function of the depth $z = z_o$, its shape will not alter very much with depth. In practice the point-spread function can by used for a broad depth range. As a consequence, the point-spread function $s_{z_o}(x, y, t)$ can by considered as space invariant. Hence the migrated image $M(x, y, t)$ can be found by:

$$M(x, y, t) \cong V_{rec}(x, y, t) \otimes^{-1} s_{z_o}(x, y, t) \tag{9}$$

Where z_o is chosen to be the most likely depth for an object. In the application of demining, z_o is taken 6 cm. The deconvolution in (9) is performed in the frequency-wavenumber domain, using a Weiner filter, which makes the migration scheme very simple and not computational intensive.

Fig. 9, 10 and 11 show the results of the migration method on data taken by the UWB GPR. The first figure represents a PMN mine buried at 5 cm of depth in sand. Fig. 10 represents a brick of dimensions 15*9*6 cm buried at the same depth, and the last figure shows a piece of 20 cm barbed wire. The 3D representation on the figures is obtained by first performing an Hilbert transform on the A-scan to find the envelope of each A-scan. Then the data is plotted by an iso-surface 3D plot, highlighting all the pixel of a given intensity. In each figure, the raw data is represented on the left. On the right, the migrated image is shown. For clarity, the ground reflection is omitted in figure 10 and 11. Although it might not be so clear on the plots, looking on the objects from above, the round shape of the PMN mine becomes very clear, whereas the shape of the brick is more rectangular. The shape of the barbed wire in Fig. 11b can be easily distinguished from the other two shapes and even contains the three sets of pins, present on the real wire. These three examples show that it is possible to extract the shape of a buried object out of the data collected by the UWB GPR.
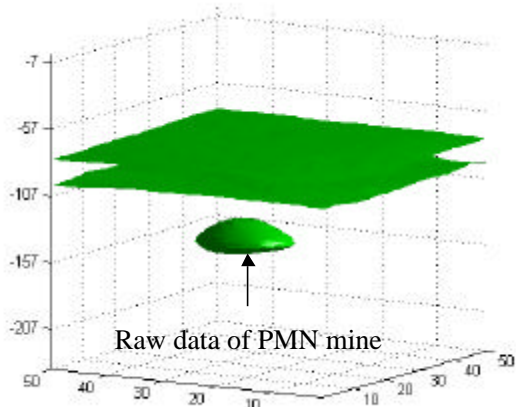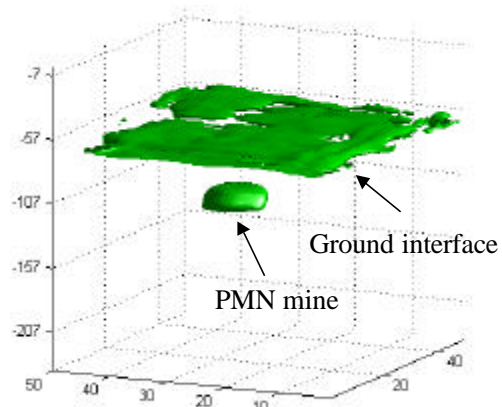
Fig.9a: Raw data of PMN mine
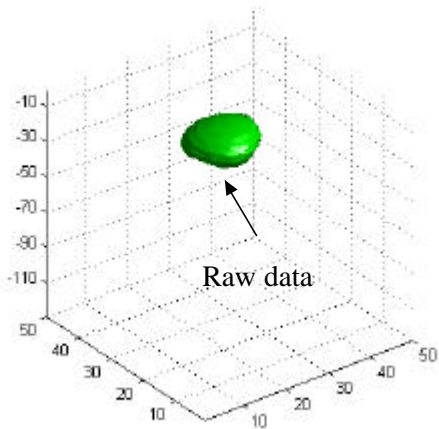

Fig.9b: Migrated image of PMN mine

Fig.10a: Raw data of brick (15*9*6cm)
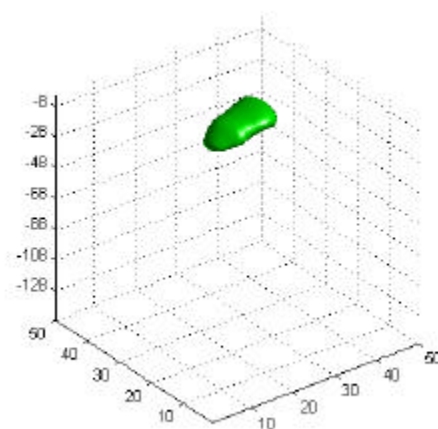

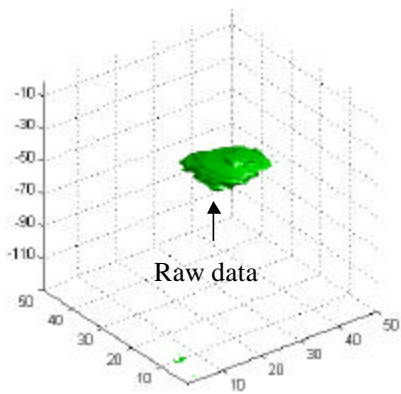Fig.10b: Migrated image of brick

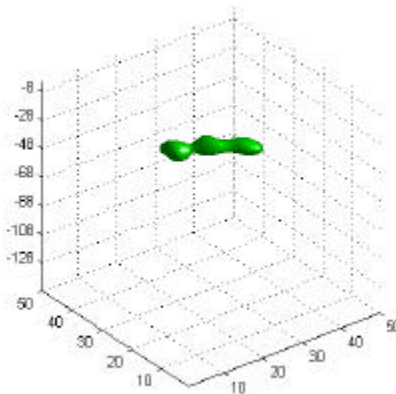Fig.11a: Raw data of piece of barbed wire (20cm)

Fig.11b: Migrated image of barbed wire

6. CONCLUSIONS

In our research on the detection and classification of plastic AP mines by means of UWB GPRs, we built a relatively simple UWB system to study its advantages and shortcomings. The main effort was put in the development of the UWB antennas, that can be used off-ground. Indoor tests revealed the capability of detecting shallow buried mines. When mines are buried deeper and the soil has a high attenuation the detection becomes almost impossible. Because of the low Q factor of the targets it is hard to extract robust features out of the A-scan, even for an UWB system. We therefore oriented our work on C-scans in order to extract the shape of the buried objects.

Disposing of an accurate time-domain model of the system turns out to be essential for predicting system performances and is useful for enhancing signal processing algorithms. The modelling is done by considering the system as a cascade of linear responses. An important part in this cascade is the modelling of the antennas by their normalised impulse response. The advantage of using the normalised IR is that the time-domain antenna equations become very simple and accurate to use. We developed the radar range equation directly in the time-domain. The range performance of the UWB GPR could thereby be expressed as a function of minimal detectable peak amplitude of our receiver and not in terms of a frequency depending signal power as in the standard radar range equation. It is seen that the range performance decreases dramatically with moisture. The time-domain model is also used to optimise the antennas offset angle. The optimal offset angle is the one that focuses the antennas on the target. In this paper we also presented a migration technique for extracting the shape of the objects out of the 3D recorded data. The migration is based on the space-time deconvolution of the collected data and the calculated point-spread function. The method takes into account the characteristics of the radar system and is not computational intensive. The quality of the 3D migrated image is good, and the results show that the discrimination of different buried objects by their shape has a potential.

7. REFERENCES

1. Scheers, B., Piette, M., Vander Vorst, A., 2000. Development of Dielectric-Filled TEM Horn Antennas for UWB GPR, submitted to *IEEE AP-2000 conference*, Switzerland, April 2000.

2. Rumsey,V., 1966. *Frequency independent antennas,* Academic Press Inc, New York, USA.

3. Farr, E.G., Baum, C.E., 1998. Time Domain Characterization of Antennas with TEM Feeds, Sensor and Simulation Notes , note 426, Air Force Research Laboratory, USA.

4. Scheers, B., Acheroy, M., Vander Vorst, A., 2000. Time Domain Simulation and Characterisation of TEM Horns Using Normalised Impulse Response, submitted to *IEE Proceedings - Microwaves, Antennas and Propagation.*

5. Yilmaz, O., 1987. *Seismic data processing*, Society of Exploration Geophysicists, Tusla, OK.

6. Berkhout, A. J., 1981. Wave field extrapolation techniques in seismic migration, a tutorial, *Geophysics*, 46, pp. 1638-1656.